Heliyon 10 (2024) e36091

Contents lists available at ScienceDirect

Heliyon

journal homepage: www.cell.com/heliyon

Research article

Electrospun poly(lactic acid) membranes with defined pore size to enhance cell infiltration

Tânia Vieira [a,b], Ana Filipa Afonso [a,b,1], Catarina Correia [a,b,1], Célia Henriques [a,b], João Paulo Borges [a,c], Jorge Carvalho Silva [a,b,*]

[a] Centro de Investigação de Materiais, Institute for Nanostructures, Nanomodelling and Nanofabrication, CENIMAT-I3N, Portugal
[b] Departamento de Física, Faculdade de Ciências e Tecnologia, Universidade Nova de Lisboa, 2829-516, Caparica, Portugal
[c] Departamento de Ciência dos Materiais, Faculdade de Ciências e Tecnologia, Universidade Nova de Lisboa, 2829-516, Caparica, Portugal

ARTICLE INFO

Keywords:
Electrospinning
Poly(lactic acid)
Fibroblasts
Cell infiltration
Macrophages

ABSTRACT

Electrospun membranes are compact structures with small pore sizes that hinder cell infiltration, resulting in membranes with cells attached only to the external surface rather than throughout the entire volume. Thus, there is a need to increase the pore size of electrospun membranes maintaining their structural similarity to the extracellular matrix. In this work, we used glucose crystals embedded in polyethylene oxide (PEO) fibers to create large pores in poly(lactic acid) (PLA) electrospun membranes to allow for cellular infiltration. The PEO fibers containing glucose crystals of different sizes (>50, 50–100 and 100–150 μm) and in varying concentrations (10, 15 and 20 %) were co-electrospun with PLA fibers and subsequently leached out using distilled water. PLA fibrous membranes without glucose crystals were also produced as controls. The membranes were examined for their morphology, mechanical properties, and potential to support the proliferation of fibroblasts. In addition, the immune response to the membranes was evaluated using monocyte-derived macrophages. The glucose crystals were uniformly distributed in the PLA membranes and their removal created open pores without collapsing the structure. Although a reduced Young's modulus was observed for membranes produced using higher glucose crystal concentrations and larger crystal sizes, the structural integrity remained intact, and the values are still suitable for tissue engineering. *In vitro* results showed that the scaffolds supported the adhesion and proliferation of fibroblasts and the pores created in the PLAmembranes were large enough for fibroblasts infiltration and colonization of the entire scaffold without inducing an inflammatory response.

1. Introduction

In tissue engineering, scaffolds are combined with cells to repair damaged tissues and organs [1]. Different techniques can be used in the production of scaffolds, such as freeze-drying, 3D-printing, phase-separation, solvent casting, and electrospinning [2].

Electrospinning is a widely used technique for producing membranes that structurally resemble the extracellular matrix (ECM) of connective tissues [3]. These scaffolds also have high porosity and surface area-to-volume ratio and provide a suitable topography for

* Corresponding author. Departamento de Física, Faculdade de Ciências e Tecnologia, Universidade Nova de Lisboa 2829-516 Caparica, Portugal.
E-mail addresses: ts.vieira@fct.unl.pt (T. Vieira), jcs@fct.unl.pt (J.C. Silva).
[1] The authors contributed equally to the work.

https://doi.org/10.1016/j.heliyon.2024.e36091
Received 27 May 2024; Received in revised form 8 August 2024; Accepted 9 August 2024
Available online 14 August 2024

cell adhesion and proliferation, favoring cellular regeneration [4].

Electrospinning has been applied to different tissues such as skin [3], bone [5], cartilage [6,7], vascular [8], cardiac [9,10] and nervous [11,12]. However, due to the continuous deposition of ultra-fine fibers, the resulting membranes are flat structures with relatively small pores and high packing density of the fibers that prevent cellular infiltration and, consequently, new tissue ingrowth [13].

To increase the pore size of the electrospun membranes, different methods have been used to adjust pore size and packing density, such as: electrospinning with salt leaching, cryogenic electrospinning, sacrificial fibers, combination of nanofibers and microfibers, ultrasonication, electrospinning using a liquid bath collector, electrospinning with gas foaming, electrospinning with electrospray and custom-made collectors. These methods have been described and discussed in detail in several reviews [14–19]. When sacrificial polymers or particles are used, a homogeneous distribution must be obtained to prevent an irregular distribution of pores and ensure pore interconnectivity [20]. The most commonly used sacrificial agent is poly(ethylene oxide) (PEO), due to its high solubility in water and its electrospinnability [21]. Other studies used co-electrospinning of PEO solutions with polycaprolactone (PCL) [22] or performed electrospraying coupled with the electrospinning of PCL, polyglycolic acid or poly (lactic-*co*-glycolic) acid to form microparticles that can be leached out, thereby facilitating the creation of open pores [23]. A straightforward approach directly introduced particles, such as salt or sugar, by placing a dispensing unit above the collector while performing fiber deposition. For example, Park et al. expanded the pore size of silk-fibroin scaffolds by adding salt particles that were released from a rotating cylinder above the collector [24]. However the resulting structure had poor mechanical properties and most of the salt crystals were not incorporated in the membranes.

Polylactic acid (PLA) is an aliphatic polyester produced from natural resources, unlike PCL, which is petrol based [25]. PLA is biodegradable, biocompatible and has been shown to induce a low inflammatory response [26]. Studies have used PLA electrospun fibers for several tissue engineering applications but only a few considered the pore dimension and the production of a three-dimensional scaffold. Shim et al. used a simple technique of mechanical expansion to produce PLA fibrous membranes with expanded pores [27]. Recently, Jing et al., 2019 used electrospinning to produce PLA membranes that were wetted by ethanol saturated CO_2 to create soft continuous nanofibrous structures [28]. However, none of these studies characterized the mechanical properties of the scaffolds to evaluate if the structural integrity was compromised.

In this study, we used PEO fibers as a vehicle to transport glucose crystals with controlled size, which were co-electrospun with PLA. These crystals were then removed to create membranes with large pores. Membranes were produced using glucose crystals with sizes in different ranges (<50, 50–100 and 100–150 μm) loaded in the PEO solution at different concentrations (10, 15 and 20 %). The mechanical properties, porosity, pore size and biocompatibility using fibroblasts and monocytes were evaluated and compared with PLA membranes obtained via standard electrospinning.

2. Materials and methods

2.1. Scaffolds fabrication

2.1.1. Solution preparation

PLA Luminy® L175 from Carbion ($M_w = 1.63 \times 10^5$ kDa) at a concentration of 6.7 wt% was dissolved in a solvent mixture of chloroform and N,N-dimethylformamide, both from Carlo Erba, at a 82:18 ratio under magnetic stirring overnight.

A solution of polyethylene oxide (PEO, Mw = 100 kDa, Sigma-Aldrich) was prepared in chloroform at a concentration of 10 % (m/m). The solution was stirred overnight. Glucose granules were sieved using a sieve agitator (AS 300 control of Retsch) to separate the granules according to their size: <50 μm, 50–100 μm and 100–150 μm. The granules with different sizes were dispersed in the PEO solution at a concentration of 10 % under magnetic stirring for 30 min before the electrospinning process. Additionally, glucose granules with a size of 100–150 μm were dispersed in the PEO solution at concentrations of 15 % and 20 %.

2.2. Electrospinning process

For the electrospinning of PLA, the PLA solution was loaded into a 5 mL plastic syringe connected to a 21 G stainless steel blunt needle (internal diameter of 0.508 mm) and placed in a syringe pump (SyringePump NE-300) that pumped the solution at a flow rate of

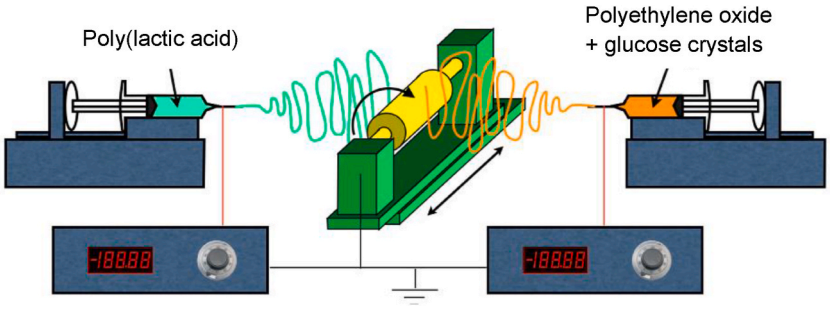

Fig. 1. – Schematic representation of the electrospinning setup.

0.8 mL/h. To the needle, a 12 kV voltage was applied using a high voltage power supply (Iseg T1 CP300 304p). A homemade cylindrical mandrel with a diameter of 8 cm, grounded and with rotational and translational motions, covered with aluminum foil, was kept at a distance of 20 cm from the needle tip and used to collect the fibers.

To produce PLA membranes with expanded pores, the co-electrospinning of PLA fibers with PEO fibers embedded with glucose crystals was performed. To do that, the PLA and PEO with glucose solutions were co-electrospun in a 180-degree geometry using a syringe pump on each side of the cylindrical mandrel (Fig. 1). The PLA solution was placed in 5 mL plastic syringes and electrospun with the following parameters: a flow rate of 0.8 mL/h, a 21 G stainless steel blunt needle, a voltage of 12 kV applied to the needle and a needle tip to collector distance of 20 cm. The PEO solution with glucose crystals was also placed in a 5 mL plastic syringe and electrospun with the following parameters: a flow rate of 0.3 mL/h, a 19 G (internal diameter 0.686 mm) stainless steel blunt needle, a voltage of 18 kV applied to the needle and a needle tip to collector distance of 25 cm.

The resulting membranes were left to dry under vacuum for 48 h to ensure solvent removal. Then, they were immersed in ethanol for 3h to wet the fibers and to allow water to penetrate inside the membrane. This was followed by immersion in distilled water for 24h with three water changes. Before freezing the samples at – 80 °C for 24h, they were observed under an optical microscope to confirm the absence of glucose granules, Finally, the samples were freeze-dried using a VacO2 system for an additional 24h.

3. Characterization

3.1. Scanning Electron Microscopy (SEM)

The morphology of the fibrous membranes was assessed using a Hitachi TM3030 Plus Electron Microscope operating in high vacuum at 15 kV. Before observation, samples were sputter coated with iridium. The ImageJ software (National Institute of Health, USA) [29] was used to measure the diameter of the fibers, analyzing at least 100 fibers. The results are expressed as the average ± experimental standard deviation. The area of the pores, as well as the Feret's diameter of the membranes was also determined using the ImageJ software according to You et al. [30] and Huang et al. [31], respectively.

3.2. Porosity measurements

The porosity of the different PLA membranes was estimated using the method described by Jung Bok Lee et al. [32]. Briefly, at least 6 samples from each PLA membrane, cut using a 15 mm circular punch, were weighed to determine the scaffold mass (g). Their dimensions were measured, with membrane thickness determined using a digital micrometer and area calculated based on the circle's area, to obtain the apparent density according to equation (1):

$$\textit{Apparent density}\ \left(\mathrm{g}\,/\,\mathrm{cm}^3\right) = \frac{\textit{scaffold mass}\ (\mathrm{g})}{\textit{scaffold thickness}\ (\mathrm{cm}) \times \textit{scaffold area}\ (\mathrm{cm}^2)} \tag{1}$$

The porosity was obtained from the ratio of the apparent and bulk densities of PLA (bulk density: 1.24 g/cm^3) according to equation (2):

$$\textit{Scaffold porosity} = 1 - \frac{\textit{scaffold apparent density}\ \left(\frac{\mathrm{g}}{\mathrm{cm}^3}\right)}{\textit{scaffold bulk density}\ \left(\frac{\mathrm{g}}{\mathrm{cm}^3}\right)} \times 100\ (\%) \tag{2}$$

Mechanical characterization.

Uniaxial tensile tests of the PLA membranes were performed using a test machine from Reometric Scientific. The area of each sample was 30 × 10 mm^2 and the membrane's thickness was in the range from 80 μm to 140 μm, measured with a digital micrometer (Mitutoyo Corporation, Japan). Samples were stretched using a 20 N load cell and an elongation speed of 2 mm/min at room temperature. At least 12 samples from three different electrospun membranes were used. The slope of the linear region of the stress-strain curve reveals the Young's modulus.

Degradation tests.

Hydrolytic degradation of the PLA fibrous membranes was carried out using phosphate buffer saline (PBS, pH 7.4 ± 0.2) solution with 0.02 % w/v sodium azide (Merck, to prevent contamination by gram-negative bacteria). The initial weight (*Wi*) of 5 samples was measured for each condition and the samples were immersed in 5 mL of PBS and incubated at 37 °C for 24 weeks. At different time points (1d, 1w, 2w, 4w, 8w, 12w and 24w), the samples were removed from the degradation medium, washed 3 times with distilled water and dried in an incubator at 37 °C for 48 h. The dried samples were weighed (*Wk*), the scaffold remaining weight was determined according to equation (3) and the results were expressed as the average ± experimental standard deviation [33].

$$\textit{Remaining weight} = 1 - \frac{Wi - Wk}{Wi} \tag{3}$$

After 8 weeks, degraded samples were observed by SEM according to the procedure previously described.

3.3. Biocompatibility evaluation of fibrous membranes

3.3.1. Cell culture

Human fetal foreskin fibroblasts (HFFF2 cell line, ECACC, UK), were cultured in complete Dulbecco's modified Eagle's medium (DMEM, Biowest) with 10 % fetal bovine serum (FBS, Biowest) and 1 % penicillin/streptomycin (Gibco).

A human monocyte cell line (THP-1 cells, ATCC, UK) was cultured in RPMI-1640 with stable glutamine (Biowest) supplemented with 10 % heat inactivated FBS (Biowest), 1 % penicillin/streptomycin (Gibco), and 1 % non-essential amino acids (Gibco). Both cell types were maintained at 37 °C in a humidified 5 % CO_2 incubator.

Samples for cell culture were cut using a 12 mm circular punch, sterilized using 70 % ethanol for 30 min, allowed to dry for 24 h, and then incubated with complete culture media overnight at 37 °C and 5 % CO_2. HFFF2 cells and THP-1 cells were seeded at a density of 20×10^3 cells/cm^2 and 80×10^3 cells/cm^2, respectively, over a 0.5 cm^2 area on each sample held by homemade Teflon inserts that were placed inside 24-well tissue culture plates. For cell controls, cells were seeded directly onto the tissue culture plate. For THP-1 cells, 8 nM of phorbol 12-myristate 13-acetate (PMA) dissolved in DMSO was added to the culture medium before cell seeding to stimulate the differentiation of monocytes into macrophages. After 48 h, the PMA containing medium was replaced with fresh complete culture medium without PMA.

3.3.2. Viability test

A resazurin (Alfa Aesar) solution (0.04 mg/mL in PBS) was used to evaluate the viability of the cells. Resazurin, which has an absorbance maximum at 600 nm, is reduced to resorufin, which has an absorbance maximum at 570 nm, by viable cells. On different days (1, 3, 5, 7, 10 and 14 for HFFF2 and 2, 4, and 7 for THP-1), the culture media were replaced by complete medium supplemented with 50 % of the resazurin solution. Wells without cells were filled with this medium and used as reference. Five replicates were performed for each experimental condition. The plates were incubated for 3 h in the CO_2 incubator and then the medium absorbance was measured at 570 nm and 600 nm using a Biotex ELX 800UV microplate reader. The cell viability is proportional to the corrected absorbance, which was obtained by subtracting the absorbance measured at 600 nm from the one measured at 570 nm and subtracting the absorbance of the medium control. Analysis of variance (ANOVA) was performed using the OriginPro 2018 software to determine the significance of differences between samples. For multiple comparisons, Tukey's test was used, and the differences were assumed to be statistically significant if $p < 0.05$.

3.3.3. Phalloidin and DAPI staining

After 2 days for THP-1 cells and 5 days for HFFF2 cells, the different PLA samples were fixed with 3.7 % formaldehyde and permeabilized with 0.5 % Triton X-100 in PBS. To observe the actin cytoskeleton and the nuclei, cells were stained with Actin-stain 555 Phalloidin (100 nM in PBS) (Cytoskeleton, Inc.) for 60 min and with DAPI (300 nM in PBS) (Molecular Probes) for 5 min, respectively. All samples were mounted on glass coverslips with mounting media (Mowiol from Sigma-Aldrich) and imaged with an epi-fluorescence microscope Nikon Eclipse Ti–S equipped with a Nikon D610 digital camera.

4. Results and discussion

4.1. Membranes characterization

Electrospinning was used to produce regular fibers with smooth surfaces. To increase the pore size of the electrospun PLA

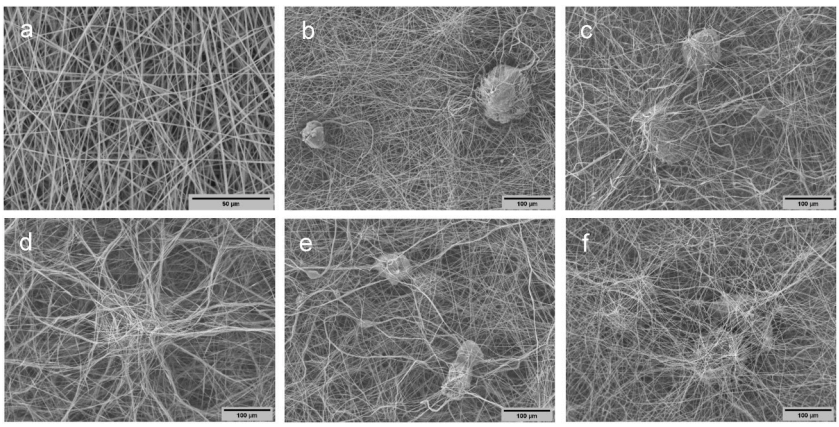

Fig. 2. – Scanning Electron Microscopy images of electrospun PLA fibers and PLA fibers co-electrospun with PEO fibers loaded with glucose crystals of different sizes: (a) membranes without glucose and PEO; (b) membranes with 10 % of glucose crystals with <50 μm; (c) membranes with 10 % of glucose crystals with 50–100 μm; (d) membranes with 10 % of glucose crystals with 100–150 μm; (e) membranes with 15 % glucose crystals with 100–150 μm and (f) membranes with 20 % glucose crystals with 100–150 μm. Scale bars: 50 μm (a) and 100 μm (b–f).

membranes, the PLA solution was co-electrospun with a PEO solution containing glucose crystals with sizes of three different ranges. The morphology of the membranes after electrospinning was analyzed by SEM, as depicted in Fig. 2. Both the glucose crystals and the PEO fibers leached out from the membranes using distilled water, creating voids in the membranes, as observed by the SEM images represented in Fig. 3. The standard PLA membranes were also submitted to the same procedure for comparison purposes. To prevent the loss of bulk volume after removing the porogens and drying the membranes, they were freeze-dried to preserve the voids created by the porogens removal, maintaining structural stability. The membranes presented a less compact structure with larger pore size compared to the standard PLA membranes. It was also possible to observe larger voids in membranes where larger glucose crystals were used. Additionally, after removal of the sacrificial agent, wider pore area and pore size dispersion were measured in the PLA membranes that contained larger glucose crystals in concentrations of 10 % and 15 % (PLA 100–150 and PLA15 100–150, Fig. 4). The small pores characteristic of standard electrospun membranes were present in the structure of all membranes. Additionally, it was observed that increasing the quantity or size of granules deposited in the PLA membrane did not affect the random fiber orientation, and the membranes maintained their structure. The average fiber diameter was similar among all membranes but those that were co-electrospun with PEO and glucose crystals presented a wider fiber diameter distribution, featuring both thinner and larger fibers compared to standard PLA (Fig. 3). Despite the clear evidence of large pores in the membranes after removal of the porogens, the bulk porosity of the membranes did not change significantly. The porosity of the PLA membranes was 90 %, while the porosity of the PLA membranes after leaching out the crystals ranged between 85 and 88 % (Table 1).

Tensile stress-strain tests were performed on the PLA fibrous membranes after removing the porogens to evaluate the effect of the open pores on the mechanical performance of the membranes. In Table 1, the mechanical properties are reported, namely, the Young's Modulus, the ultimate tensile strength and the elongation at break. A representative stress-strain curve for each PLA membrane is

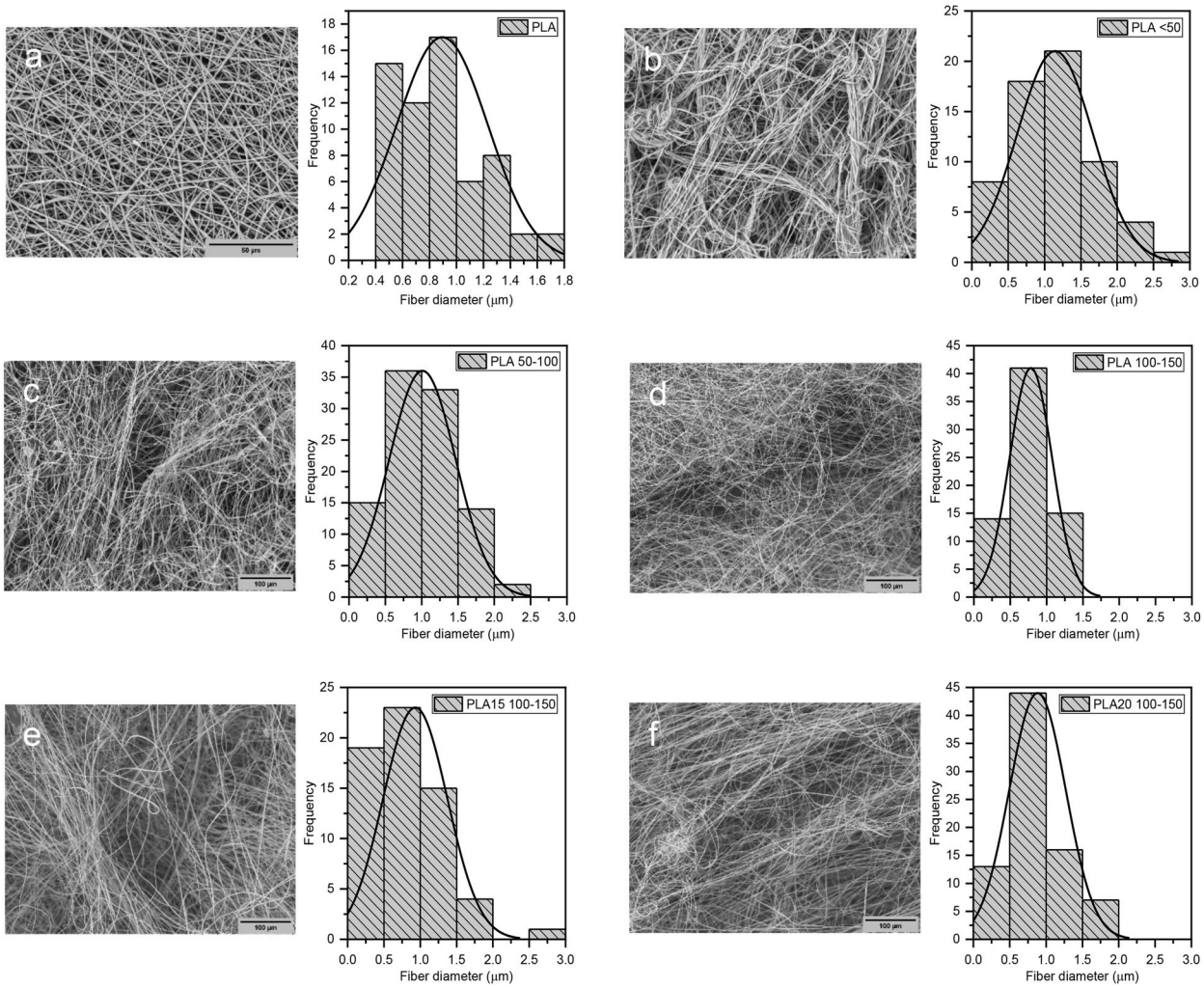

Fig. 3. – Scanning Electron Microscopy images of electrospun PLA fibers after leaching out the PEO and glucose crystals and their respective fiber diameter histograms. (a) PLA fibers; PLA fibers co-electrospun with PEO fibers loaded with glucose crystals of different sizes: (b) 10 %, <50 μm; (c) 10 %, 50–100 μm; (d) 10 %, 100–150 μm; (e) 15 %, 100–150 μm and (f) 20 %, 100–150 μm.

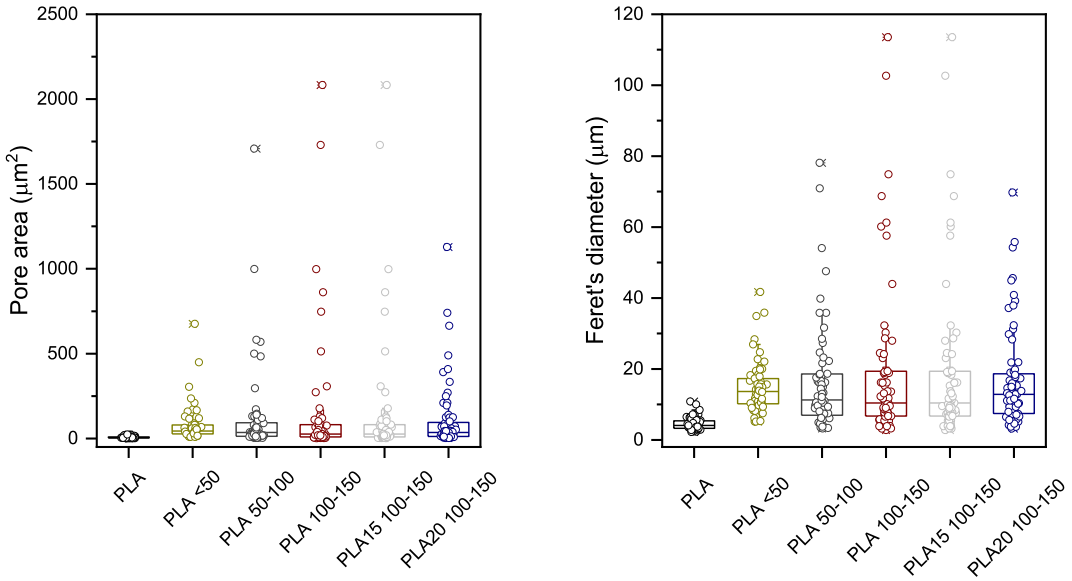

Fig. 4. – Area (μm^2) and Feret's diameter (μm) of the pores for the different PLA membranes.

shown in Fig. 5. The standard PLA membranes presented a Young's modulus of 15 ± 3 MPa. The Young's modulus of PLA fibers produced using electrospinning depends on the fiber's characteristics such as fiber diameter and orientation. According to Shi et al. [34], the mechanical properties of PLA fibrous membranes obtained by electrospinning were smaller than the Young's modulus of the standard PLA membranes produced in the present study. This difference can be related to the average fiber diameter of the PLA fibers obtained in this study, which was smaller when compared to the average diameter of the PLA fibers produced in the study performed by Shi et al. Another factor that affects the mechanical properties of the PLA membranes is the treatment of the membranes with ethanol to remove the PEO fibers and the glucose crystals. According to Pavlova et al., 2019 [35], ethanol has a plasticizer effect on PLA membranes. In their work, after drying the ethanol treated PLA membranes, they observed membranes with higher elongation at break and higher Young's modulus.

The PLA membranes, after removing glucose grains of dimensions smaller than 100 μm, showed a slightly reduced Young's modulus when compared to standard PLA membranes. The values of elongation at break and the ultimate tensile strength were similar between the PLA membranes and the membranes where glucose crystals with dimensions inferior to 100 μm were leached out. However, when glucose crystals with sizes between 100 and 150 μm were removed from PLA membranes, a significant reduction of Young's modulus and ultimate tensile strength as well as an increase in the elongation at break were observed when compared to the standard PLA membranes. Thus, the use of large crystals created voids large enough to significantly affect the mechanical properties of the membranes. A linear relationship between the decrease of tensile strength and stiffness with the presence of sacrificial PEO fibers was observed before by Baker et al. [36] and Voorneveld et al. [37]. The decrease in the Young's modulus should be even more pronounced in our study due to the additional removal of the glucose crystals, particularly the ones with larger sizes. Soft tissues in the human body present Young's moduli ranging from 0.01 MPa to 15 MPa [38]. The Young's modulus of human skin, which depends on the skin source and the age, varies from 0.10 MPa in the initial slope of the stress-strain curves (up to 40 % stretching) and up to 18.8 MPa in the high strain-region [39]. In the study developed by Zahouani et al., the mechanical properties of the dermis as well as dermis equivalents were determined to be 8 kPa [40]. Despite the significant reduction of the Young's modulus of the PLA membranes after leaching, they still have mechanical properties suitable for being applied as skin substitutes.

The degradation of the PLA electrospun membranes was determined by measuring the weight changes of the PLA membranes over 24 weeks in PBS at 37 °C. PLA is degraded by hydrolysis of the ester-bond backbone, which occurs by surface or bulk erosion and

Table 1
– Results of porosity analysis and tensile tests of PLA fibrous membranes. Ultimate tensile strength, σ, Young's modulus, Y, and strain at break, ε (mean ± experimental standard deviation).

Fibrous membrane	Porosity (%)	Mechanical testing		
		Y (MPa)	σ (MPa)	ε (%)
PLA	90 ± 2	15 ± 3	1.4 ± 0.3	61 ± 9
PLA <50 μm	87 ± 2	10 ± 4	1.3 ± 0.4	72 ± 6
PLA 50–100 μm	88 ± 2	14 ± 3	1.2 ± 0.3	52 ± 9
PLA 100–150 μm	85 ± 2	5 ± 2	1.3 ± 0.3	91 ± 8
PLA15 100–150 μm	86 ± 2	3 ± 1	0.9 ± 0.2	115 ± 14
PLA20 100–150 μm	88 ± 1	4 ± 1	0.9 ± 0.1	106 ± 14

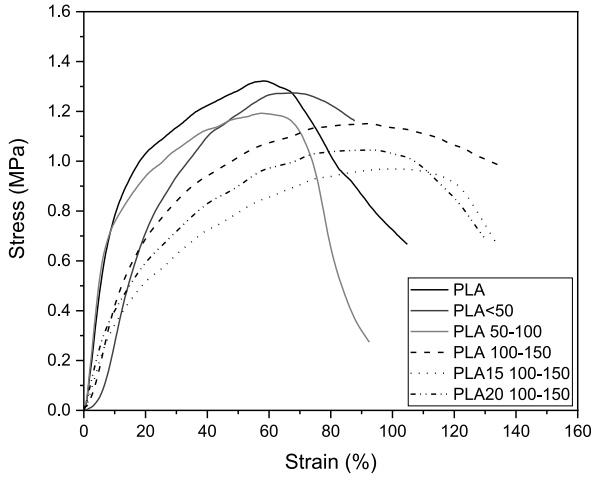

Fig. 5. – Typical stress-strain curves of the electrospun PLA membranes after removing the glucose crystals.

results in monomers and oligomers of lactic acid [41,42]. The degradation profiles of the PLA membranes are shown in Fig. 6a. After removing the porogens, the membranes barely lose weight over 24 weeks, independently of the structure of the membrane (quantity and dimension of porogen). A similar result was obtained by Dias et al. who showed that PLA electrospun membranes barely lost weight over the period of 20 weeks [43]. SEM images were also acquired after that period to evaluate the morphological changes (Fig. 6b–g). The structure of the membranes was slightly compromised as can be observed in the SEM images, with visible rupture of some fibers. However, their smooth morphology was maintained. The increase in the membrane pore size caused by the removal of glucose crystals and PEO did not negatively affect the degradation rate of PLA electrospun membranes over a period of up to 24 weeks. When this type of scaffold is used for wound healing applications, PLA persists in the body for at least 12 months, providing sufficient time for dermal remodeling and new tissue formation [44].

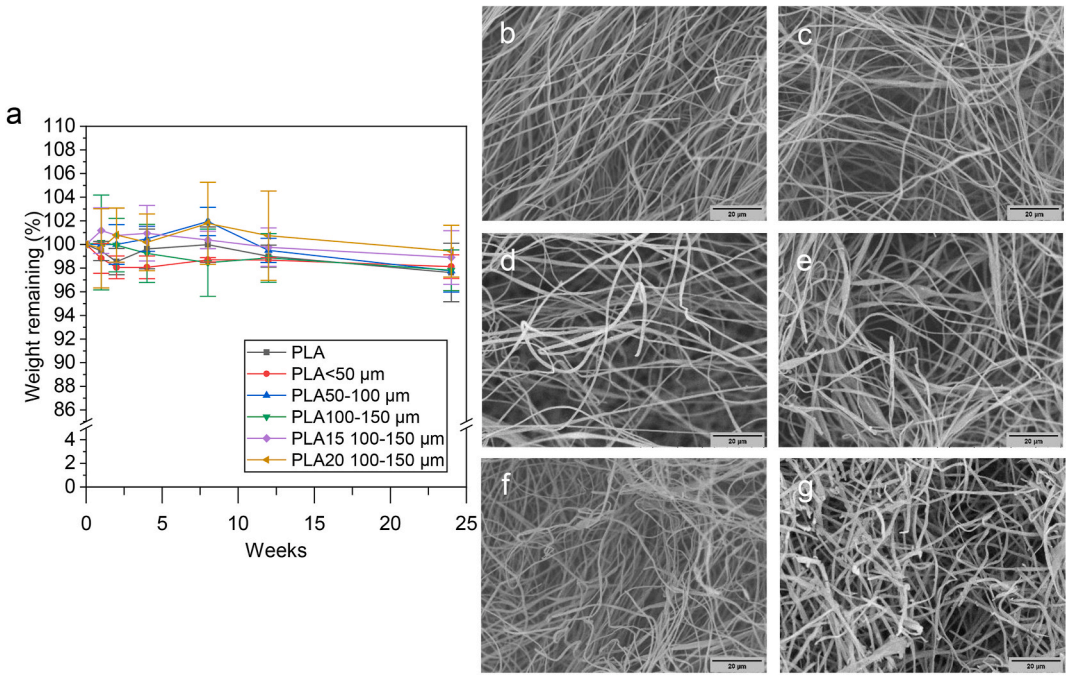

Fig. 6. – (a) Hydrolytic degradation of electrospun PLA membranes immersed in PBS during 24 weeks. Scanning Electron Microscopy images of electrospun fibers after immersion in PBS during 24 weeks: PLA fibers (b) and PLA fibers co-electrospun with PEO fibers loaded with glucose crystals of different sizes: (c) 10 %, <50 µm; (d) 10 %, 50–100 µm; (e) 10 %, 100–150 µm; (f) 15 %, 100–150 µm and (g) 20 %, 100–150 µm.

4.2. In vitro evaluation

The viability of HFFF2 cells seeded on PLA membranes was evaluated using the resazurin assay over a period of 14 days. The resazurin assay measures the metabolic activity of cells, which is assumed to be proportional to the number of cells. The cell population results are shown in Fig. 7. An adhesion ratio of 56 % when compared to the cell control was observed for PLA sample. Although PLA is a biocompatible polymer, its hydrophobic nature can impair the adhesion rate of cells. The adhesion ratios for the membranes with bigger pores were smaller, revealing an increased difficulty of cells to adhere to a more open structure. The cell population increased over time for all samples but lagged the control at all time points. However, the cell proliferation rate of the PLA membranes, evaluated by the ratio between cell populations on days 14 and 1, was similar to the cell control when compared to the PLA membranes with larger pores, as presented in Table 2. Confluence was reached faster in cell controls and then in PLA membranes without large pores, suggesting a delayed proliferation in the membranes with larger pores. This happens despite the higher similarity of electrospun membranes with the extracellular matrix, where the cells need more time to establish contact points and reach confluence, which was also previously reported by Querido et al. [45], Jiang et al. [46], and Chang et al. [47].

The cytoskeleton and the nuclei of the cells were stained with phalloidin and DAPI, respectively (Fig. 8). Differences were observed in the cells' cytoskeleton when they were seeded on membranes with different structures. The cells presented a more stretched morphology, with longer actin filaments and a larger projected area in contact with membranes with larger pores (Fig. 8d–f). It was also observed that cells spread across different planes in membranes with large pores, unlike in standard PLA membranes where cells are mainly located on the surface. The presence of large pores enables cell penetration in the *z*-plane, which allows cells to be distributed throughout the membrane. Hodge and Quint also reported an increase in cell infiltration when polyethylene oxide microparticles were used as sacrificial agents to create expanded pores in PLA electrospun membranes having pore sizes around 20 μm [23]. Other studies used cryogenic electrospinning [48,49] as a pore-enlarging strategy to obtain fibrous membranes with enlarged pores without collapsing, when compared to other porogen agents. Larger pores, with diameters of 40 μm, were created inside the electrospun membranes, allowing for cell infiltration.

It is crucial to consider the inflammatory response when developing scaffolds destined for Tissue Engineering, as it significantly affects how the body accepts the foreign material and its ability to heal successfully after implantation [50]. Electrospun membranes have been shown to influence macrophage activation and inflammatory response, which depends on fiber diameter, alignment and pore size. Fibers with large diameter [51], high degree of alignment [52] and large pore size [53] have shown the ability to induce macrophage polarization towards the anti-inflammatory (M2) phenotype.

THP-1 cells were cultured in the presence of the PLA membranes to evaluate their effect on immune response modulation. When THP-1 cells induced by PMA to differentiate into macrophages were seeded on the PLA membranes, their adhesion was higher for the standard PLA membranes, even when compared to the cell control, and decreased for membranes with larger pores (Fig. 9). Additionally, the cellular metabolic activity reduced as a function of culture time while the cells seeded on the well plates (cell control) exhibited unaffected metabolic activity over time. The absence of a strong metabolic activity suggests that the fibrous membranes do not activate the macrophages into the pro-inflammatory (M1) phenotype [54]. Similar results were obtained previously by Fuller et al., 2016 [55] who found a reduced metabolic activity of macrophage derived THP-1 monocytes in polycaprolactone electrospun membranes over time. Our results suggest that the fibrous membranes can modulate the immune response towards the anti-inflammatory phenotype.

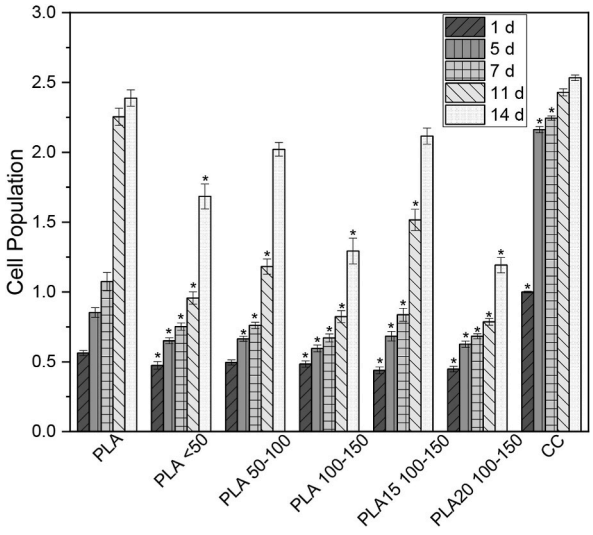

Fig. 7. – HFFF2 cell population on PLA membranes after removing the glucose crystals and on tissue culture plastic wells (CC) determined using the resazurin assay on days 1, 5, 7, 11 and 14 (mean ± standard deviation, $n = 5$). The results were statistically compared to the PLA membranes for each time point, using ANOVA with a significance level of $p < 0.05$ (represented by an asterisk).

Table 2
– Adhesion ratio and cell proliferation evaluated by the ratio between cell populations on day 14 and on day 1 (PR14/1) of HFFF2 cells of PLA membranes with different pore sizes. Results are expressed as mean ± combined standard uncertainty.

	PLA	PLA <50 μm	PLA 50–100 μm	PLA 100–150 μm	PLA15 100–150 μm	PLA20 100–150 μm	Cell control
Adhesion ratio (%)	56 ± 2	48 ± 3	50 ± 2	49 ± 2	44 ± 3	45 ± 2	100 ± 1
PR14/1	4.2 ± 0.1	3.6 ± 0.2	4.1 ± 0.1	2.7 ± 0.2	4.8 ± 0.2	2.7 ± 0.2	2.5 ± 0.1

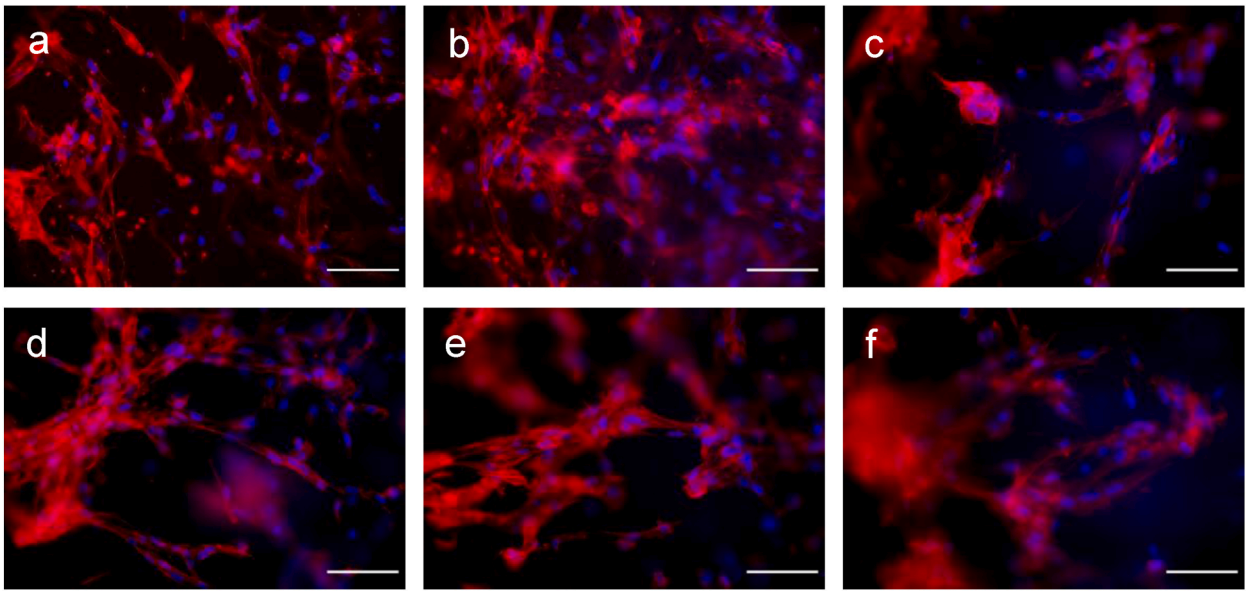

Fig. 8. – Fluorescent images of cytoskeleton (phalloidin – red) and nuclei (DAPI – blue) of HFFF2 cells at day 7 of culture seeded on PLA membranes (a) and PLA membranes co-electrospun with PEO fibers loaded with glucose crystals of different sizes: 10 %, <50 μm (b); 10 % 50–100 μm (c); 10 %, 100–150 μm (d); 15 %, 100–150 μm (e) and 20 %, 100–150 μm (f). Scale bar: 100 μm.

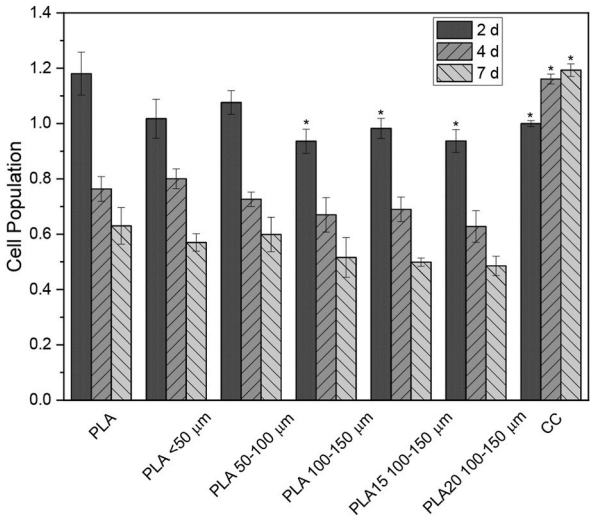

Fig. 9. – THP-1 cell population on PLA membranes after removing the glucose crystals and on TCP wells (CC) determined using the resazurin assay on days 2, 4 and 7 (mean ± standard deviation, $n = 4$). The results were statistically compared to the PLA membranes for each individual day, using ANOVA with a significance level of $p < 0.05$ (represented by an asterisk).

The representative images of the staining of macrophages cytoskeleton and nuclei with phalloidin and DAPI after 2 days and 7 days are shown in Fig. 10 and in Fig. 11, respectively. After 2 days (Fig. 10), macrophages mainly presented a rounded morphology with few protrusions, which is usually associated with a non-activated phenotype (M0) [56]. After 1 week (Fig. 11), a strong reduction in cell number was observed (visible by the reduced number of nuclei), confirming the results obtained in the resazurin assay. At this time point, macrophages presented an elongated spindle-like shape with actin filaments protruding from cells which is a characteristic of macrophages polarized to M2, as observed before by Kurynina et al. [57].

Other methods, such as cryo-electrospinning, enable the formation of porogens in situ by cooling the collector, which allows the formation of ice crystals [58,59]. By controlling the humidity, it is possible to obtain membranes with different pores sizes by varying the dimensions of the ice crystal during the electrospinning process [58,59]. In this work, we achieved fibrous membranes with various pore sizes by controlling both the size of the glucose granules and their concentration in the solution prior to the electrospinning process, without depending on the environmental conditions. With the combination of glucose crystals with PEO, which were leached out, it was possible to obtain a structure with pores suitable for the adhesion, proliferation and infiltration of fibroblasts, where the cells populate the entire scaffold and, at the same time, modulated the immune response by reducing the inflammatory activity. Membranes with different pore sizes were obtained by varying the size of the crystal granules. Furthermore, the concentration of crystals in the polymeric solution should be kept below 20 % as higher concentrations can lead to needle clogging during the electrospinning process and may cause the structure to collapse due to poor mechanical stability.

Creating a membrane with enlarged pores to allow cell infiltration is of paramount importance for creating three-dimensional structures that resemble the ECM [13]. In cases of ECM destruction, such as full-thickness wounds, the cells responsible for tissue repair cannot reach the wound site, preventing regeneration [60]. Thus, electrospun membranes with large pores that facilitate cell infiltration and mobility not only help in the regeneration process but also serve as in vitro tissue models similar to the native ECM environment, allowing for a deeper study of cell-cell and cell-ECM interactions and matrix deposition and organization [14].

5. Concluding remarks

The creation of pores large enough to allow for cell infiltration in electrospun membranes has been challenging despite the different approaches that have been used. With this study, we conclude that it is possible to regulate the pore size of PLA electrospun membranes by using glucose crystals transported by PEO as sacrificial agents. PLA was chosen because it is approved by the Food and Drug Administration, is already used in degradable sutures and does not pose any risk of disease transmission [25]. Electrospun PLA membranes accelerate wound closure in vivo when compared to traditional gauzes [61] and facilitate new tissue formation in dermal reconstruction [62]. After removing the porogens, the resulting membranes can withstand mechanical strain and maintain their porous structure without collapsing. However, the mechanical properties of the membranes still need improvements regarding the application as dermal substitutes. Membranes with large pores allowed for fibroblast infiltration with reduced inflammatory activity. Although the fibroblasts took longer to proliferate when seeded in membranes with larger pores, they infiltrated the entire membrane creating a true three-dimensional distribution resembling the ECM. Overall, the membranes produced using glucose crystals with sizes ranging from

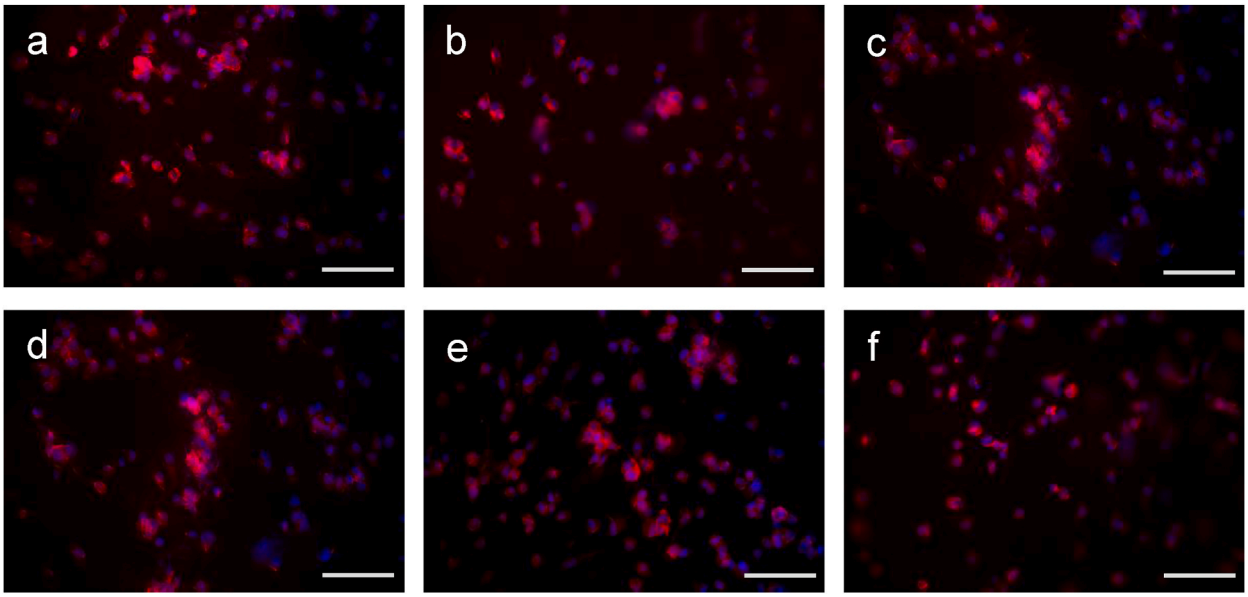

Fig. 10. – Fluorescent images of cytoskeleton (phalloidin – red) and nuclei (DAPI – blue) of THP-1 derived macrophages at day 2 of culture seeded on PLA membranes (a) and PLA membranes co-electrospun with PEO fibers loaded with glucose crystals of different sizes: 10 %, <50 μm (b); 10 %, 50–100 μm (c); 10 %, 100–150 μm (d); 15 %, 100–150 μm (e) and 20 %, 100–150 μm (f). Scale bar: 100 μm.

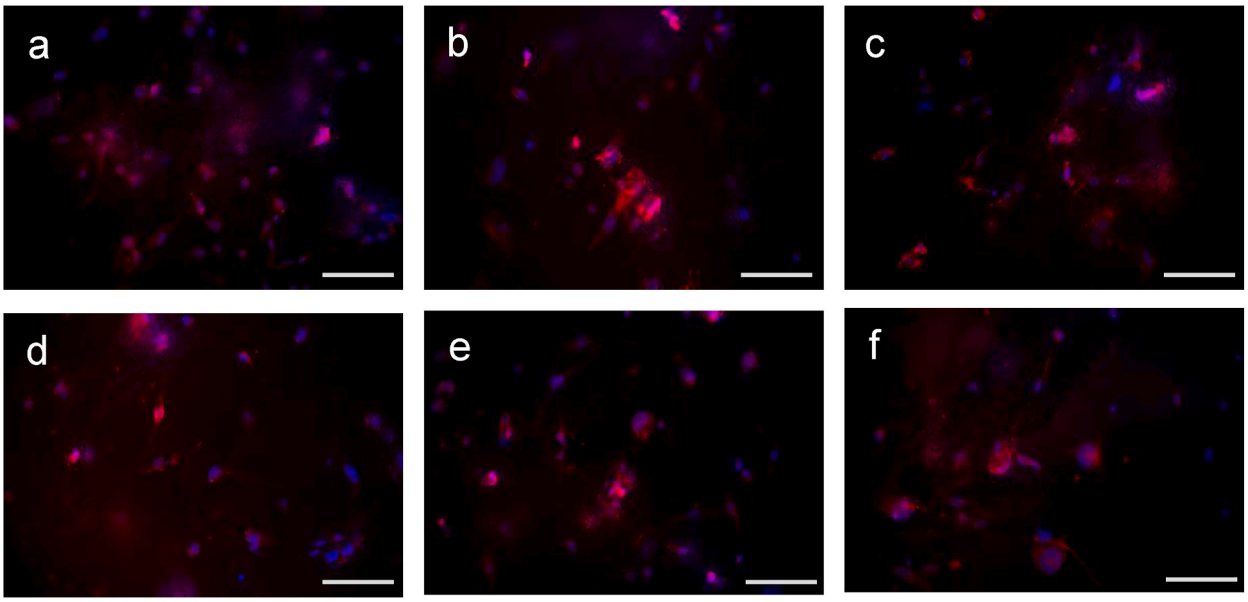

Fig. 11. – Fluorescent images of cytoskeleton (phalloidin – red) and nuclei (DAPI – blue) of THP-1 derived macrophages at day 7 of culture seeded on PLA membranes (a) and PLA membranes co-electrospun with PEO fibers loaded with glucose crystals of different sizes: 10 %, <50 μm (b); 10 %, 50–100 μm (c); 10 %, 100–150 μm (d); 15 %, 100–150 μm (e) and 20 %, 100–150 μm (f). Scale bar: 100 μm.

100 μm to 150 μm can be further explored as promising scaffolds for dermal skin tissue engineering. Next steps will include investigating the production of total collagen, given its importance for new tissue formation by cells seeded on the scaffolds.

Data availability statement

Data will be made available on request.

CRediT authorship contribution statement

Tânia Vieira: Writing – original draft, Resources, Investigation, Funding acquisition, Formal analysis, Data curation. **Ana Filipa Afonso:** Visualization, Investigation, Data curation. **Catarina Correia:** Visualization, Investigation, Data curation. **Célia Henriques:** Writing – review & editing, Resources, Formal analysis. **João Paulo Borges:** Validation, Resources, Funding acquisition. **Jorge Carvalho Silva:** Writing – review & editing, Validation, Supervision, Resources, Project administration, Funding acquisition, Conceptualization.

Declaration of competing interest

The authors declare that they have no known competing financial interests or personal relationships that could have appeared to influence the work reported in this paper.

Acknowledgments

This research was funded by the FCT-Fundação para a Ciência e a Tecnologia, I.P., in the scope of the projects 2022.07258.PTDC (123SkinHeal) and PTDC/BTM-MAT/31470/2017 (iSkin2) and the projects LA/P/0037/2020, UIDP/50025/2020 and UIDB/50025/2020 of the Associate Laboratory Institute of Nanostructures, Nanomodelling and Nanofabrication-i3N.

References

[1] A.E. Eldeeb, S. Salah, N.A. Elkasabgy, Biomaterials for tissue engineering applications and current updates in the field: a comprehensive review, AAPS PharmSciTech 23 (2022) 267, https://doi.org/10.1208/s12249-022-02419-1.
[2] M. Mabrouk, H.H. Beherei, D.B. Das, Recent progress in the fabrication techniques of 3D scaffolds for tissue engineering, Mater. Sci. Eng. C 110 (2020).
[3] A. Keirouz, M. Chung, J. Kwon, G. Fortunato, N. Radacsi, 2D and 3D electrospinning technologies for the fabrication of nanofibrous scaffolds for skin tissue engineering: a review, Wiley Interdiscip Rev Nanomed Nanobiotechnol 12 (2020).
[4] M. Rahmati, D.K. Mills, A.M. Urbanska, M.R. Saeb, J.R. Venugopal, S. Ramakrishna, M. Mozafari, Electrospinning for tissue engineering applications, Prog. Mater. Sci. 117 (2021).

[5] W. Lin, M. Chen, T. Qu, J. Li, Y. Man, Three-dimensional electrospun nanofibrous scaffolds for bone tissue engineering, J. Biomed. Mater. Res. B Appl. Biomater. 108 (2020) 1311–1321.

[6] S. Ghadirian, S. Karbasi, A.Z. Kharazi, M. Setayeshmehr, Evaluation of the effects of halloysite nanotubes on physical, mechanical, and biological properties of polyhydroxy butyrate electrospun scaffold for cartilage tissue engineering applications, J. Polym. Environ. 32 (2024) 1170–1187, https://doi.org/10.1007/s10924-023-03024-4.

[7] A.F. Girão, Â. Semitela, A.L. Pereira, A. Completo, P.A.A.P. Marques, Microfabrication of a biomimetic arcade-like electrospun scaffold for cartilage tissue engineering applications, J. Mater. Sci. Mater. Med. 31 (2020), https://doi.org/10.1007/s10856-020-06407-4.

[8] A.P. Rickel, X. Deng, D. Engebretson, Z. Hong, Electrospun nanofiber scaffold for vascular tissue engineering, Mater. Sci. Eng. C 129 (2021).

[9] N. Adadi, M. Yadid, I. Gal, M. Asulin, R. Feiner, R. Edri, T. Dvir, Electrospun fibrous PVDF-TrFe scaffolds for cardiac tissue engineering, differentiation, and maturation, Adv Mater Technol 5 (2020), https://doi.org/10.1002/admt.201900820.

[10] N. Nagiah, R. El Khoury, M.H. Othman, J. Akimoto, Y. Ito, D.A. Roberson, B. Joddar, Development and characterization of furfuryl-gelatin electrospun scaffolds for cardiac tissue engineering, ACS Omega 7 (2022) 13894–13905, https://doi.org/10.1021/acsomega.2c00271.

[11] J. Qian, Z. Lin, Y. Liu, Z. Wang, Y. Lin, C. Gong, R. Ruan, J. Zhang, H. Yang, Functionalization strategies of electrospun nanofibrous scaffolds for nerve tissue engineering, Smart Mater Med 2 (2021) 260–279.

[12] F. Zha, W. Chen, G. Lv, C. Wu, L. Hao, L. Meng, L. Zhang, D. Yu, Effects of surface condition of conductive electrospun nanofiber mats on cell behavior for nerve tissue engineering, Mater. Sci. Eng. C 120 (2021), https://doi.org/10.1016/j.msec.2020.111795.

[13] Y. Zhang, M. Zhang, D. Cheng, S. Xu, C. Du, L. Xie, W. Zhao, Applications of electrospun scaffolds with enlarged pores in tissue engineering, Biomater. Sci. 10 (2022) 1423–1447.

[14] K.P. Feltz, E.A. Growney Kalaf, C. Chen, R.S. Martin, S.A. Sell, A review of electrospinning manipulation techniques to direct fiber deposition and maximize pore size, Electrospinning 2 (2017) 46–61, https://doi.org/10.1515/esp-2017-0002.

[15] J.M. Ameer, P.R. Anil Kumar, N. Kasoju, Strategies to tune electrospun scaffold porosity for effective cell response in tissue engineering, J. Funct. Biomater. 10 (2019).

[16] J. Wu, Y. Hong, Enhancing cell infiltration of electrospun fibrous scaffolds in tissue regeneration, Bioact. Mater. 1 (2016) 56–64.

[17] J. Rnjak-Kovacina, A.S. Weiss, Increasing the pore size of electrospun scaffolds, Tissue Eng., Part B 17 (2011) 365–372, https://doi.org/10.1089/ten.teb.2011.0235.

[18] I. Jun, H.S. Han, J.R. Edwards, H. Jeon, Electrospun fibrous scaffolds for tissue engineering: viewpoints on architecture and fabrication, Int. J. Mol. Sci. 19 (2018).

[19] S. Zhong, Y. Zhang, C.T. Lim, Fabrication of large pores in electrospun nanofibrous scaffolds for cellular infiltration: a review, Tissue Eng., Part B 18 (2012) 77–87, https://doi.org/10.1089/ten.teb.2011.0390.

[20] D. Olvera, R. Schipani, B.N. Sathy, D.J. Kelly, Electrospinning of highly porous yet mechanically functional microfibrillar scaffolds at the human scale for ligament and tendon tissue engineering, Biomedical Materials (Bristol) 14 (2019), https://doi.org/10.1088/1748-605X/ab0de1.

[21] C. Henriques, R. Vidinha, D. Botequim, J.P. Borges, J.A.M.C. Silva, A systematic study of solution and processing parameters on nanofiber morphology using a new electrospinning apparatus, Proceedings of the Journal of Nanoscience and Nanotechnology 9 (June 2009) 3535–3545.

[22] N.E. Zander, J.A. Orlicki, A.M. Rawlett, T.P. Beebe, Electrospun polycaprolactone scaffolds with tailored porosity using two approaches for enhanced cellular infiltration, J. Mater. Sci. Mater. Med. 24 (2013) 179–187, https://doi.org/10.1007/s10856-012-4771-7.

[23] J. Hodge, C. Quint, The improvement of cell infiltration in an electrospun scaffold with multiple synthetic biodegradable polymers using sacrificial PEO microparticles, J. Biomed. Mater. Res. 107 (2019) 1954–1964, https://doi.org/10.1002/jbm.a.36706.

[24] Y.R. Park, H.W. Ju, J.M. Lee, D.K. Kim, O.J. Lee, B.M. Moon, H.J. Park, J.Y. Jeong, Y.K. Yeon, C.H. Park, Three-dimensional electrospun silk-fibroin nanofiber for skin tissue engineering, Int. J. Biol. Macromol. 93 (2016) 1567–1574, https://doi.org/10.1016/j.ijbiomac.2016.07.047.

[25] S. Castañeda-Rodríguez, M. González-Torres, R.M. Ribas-Aparicio, M.L. Del Prado-Audelo, G. Leyva-Gómez, E.S. Gürer, J. Sharifi-Rad, Recent advances in modified poly (lactic acid) as tissue engineering materials, J. Biol. Eng. 17 (2023).

[26] S. Liu, S. Qin, M. He, D. Zhou, Q. Qin, H. Wang, Current applications of poly(lactic acid) composites in tissue engineering and Drug delivery, Compos. B Eng. 199 (2020).

[27] I.K. Shim, M.R. Jung, K.H. Kim, Y.J. Seol, Y.J. Park, W.H. Park, S.J. Lee, Novel three-dimensional scaffolds of poly(L -lactic acid) microfibers using electrospinning and mechanical expansion: fabrication and bone regeneration, J. Biomed. Mater. Res. B Appl. Biomater. 95 (2010) 150–160, https://doi.org/10.1002/jbm.b.31695.

[28] X. Jing, H. Li, H.Y. Mi, Y.J. Liu, Y.M. Tan, Fabrication of three-dimensional fluffy nanofibrous scaffolds for tissue engineering via electrospinning and CO2 escaping foaming, Ind. Eng. Chem. Res. 58 (2019) 9412–9421, https://doi.org/10.1021/acs.iecr.9b00935.

[29] C.A. Schneider, W.S. Rasband, K.W. Eliceiri, NIH image to ImageJ: 25 Years of image analysis, Nat. Methods 9 (2012).

[30] C. You, Q. Li, X. Wang, P. Wu, J.K. Ho, R. Jin, L. Zhang, H. Shao, C. Han, Silver nanoparticle loaded collagen/chitosan scaffolds promote wound healing via regulating fibroblast migration and macrophage activation, Sci. Rep. 7 (2017), https://doi.org/10.1038/s41598-017-10481-0.

[31] L. Huang, J. Huang, H. Shao, X. Hu, C. Cao, S. Fan, L. Song, Y. Zhang, Silk scaffolds with gradient pore structure and improved cell infiltration performance, Mater. Sci. Eng. C 94 (2019) 179–189, https://doi.org/10.1016/j.msec.2018.09.034.

[32] J.B. Lee, S.I. Jeong, M.S. Bae, D.H. Yang, D.N. Heo, C.H. Kim, E. Alsberg, I.K. Kwon, Highly porous electrospun nanofibers enhanced by ultrasonication for improved cellular infiltration, Tissue Eng. 17 (2011) 2695–2702, https://doi.org/10.1089/ten.tea.2010.0709.

[33] T. Vieira, J. Carvalho Silva, A.M. Botelho do Rego, J.P. Borges, C. Henriques, Electrospun biodegradable chitosan based-poly(urethane urea) scaffolds for soft tissue engineering, Mater. Sci. Eng. C 103 (2019), https://doi.org/10.1016/j.msec.2019.109819.

[34] Q. Shi, C. Zhou, Y. Yue, W. Guo, Y. Wu, Q. Wu, Mechanical properties and in vitro degradation of electrospun bio-nanocomposite mats from PLA and cellulose nanocrystals, Carbohydr. Polym. 90 (2012) 301–308, https://doi.org/10.1016/j.carbpol.2012.05.042.

[35] E.R. Pavlova, D.V. Bagrov, K.Z. Monakhova, A.A. Piryazev, A.I. Sokolova, D.A. Ivanov, D.V. Klinov, Tuning the properties of electrospun polylactide mats by ethanol treatment, Mater. Des. 181 (2019), https://doi.org/10.1016/j.matdes.2019.108061.

[36] B.M. Baker, A.O. Gee, R.B. Metter, A.S. Nathan, R.A. Marklein, J.A. Burdick, R.L. Mauck, The potential to improve cell infiltration in composite fiber-aligned electrospun scaffolds by the selective removal of sacrificial fibers, Biomaterials 29 (2008) 2348–2358, https://doi.org/10.1016/j.biomaterials.2008.01.032.

[37] J. Voorneveld, A. Oosthuysen, T. Franz, P. Zilla, D. Bezuidenhout, Dual electrospinning with sacrificial fibers for engineered porosity and enhancement of tissue ingrowth, J. Biomed. Mater. Res. B Appl. Biomater. 105 (2017) 1559–1572, https://doi.org/10.1002/jbm.b.33695.

[38] G. Singh, A. Chanda, Mechanical properties of whole-body soft human tissues: a review, Biomedical Materials (Bristol) 16 (2021).

[39] F.H. Silver, J.W. Freeman, D. Devore, Viscoelastic properties of human skin and processed dermis, Skin Res. Technol. 7 (2001) 18–23, https://doi.org/10.1034/j.1600-0846.2001.007001018.x.

[40] H. Zahouani, C. Pailler-Mattei, B. Sohm, R. Vargiolu, V. Cenizo, R. Debret, Characterization of the mechanical properties of a dermal equivalent compared with human skin in vivo by indentation and static friction tests, Skin Res. Technol. 15 (2009) 68–76, https://doi.org/10.1111/j.1600-0846.2008.00329.x.

[41] M.A. Elsawy, K.H. Kim, J.W. Park, A. Deep, Hydrolytic degradation of polylactic acid (PLA) and its composites, Renew. Sustain. Energy Rev. 79 (2017) 1346–1352.

[42] D. da Silva, M. Kaduri, M. Poley, O. Adir, N. Krinsky, J. Shainsky-Roitman, A. Schroeder, Biocompatibility, biodegradation and excretion of polylactic acid (PLA) in medical implants and theranostic systems, Chem. Eng. J. 340 (2018) 9–14, https://doi.org/10.1016/j.cej.2018.01.010.

[43] J.C. Dias, C. Ribeiro, V. Sencadas, G. Botelho, J.L.G. Ribelles, S. Lanceros-Mendez, Influence of fiber diameter and crystallinity on the stability of electrospun poly(l-lactic acid) membranes to hydrolytic degradation, Polym. Test. 31 (2012) 770–776, https://doi.org/10.1016/j.polymertesting.2012.05.007.

[44] P. Deshpande, C. Ramachandran, V.S. Sangwan, S. MacNeil, Cultivation of Limbal Epithelial Cells on Electrospun Poly (Lactide-Co-Glycolide) Scaffolds for Delivery to the Cornea (2013) 179–185.

[45] D. Querido, T. Vieira, J.L. Ferreira, C. Henriques, J.P. Borges, J.C. Silva, Study on the incorporation of chitosan flakes in electrospun polycaprolactone scaffolds, Polymers 14 (2022), https://doi.org/10.3390/polym14081496.
[46] X. Jiang, H.Q. Cao, L.Y. Shi, S.Y. Ng, L.W. Stanton, S.Y. Chew, Nanofiber topography and sustained biochemical signaling enhance human mesenchymal stem cell neural commitment, Acta Biomater. 8 (2012) 1290–1302, https://doi.org/10.1016/j.actbio.2011.11.019.
[47] J.C. Chang, S. Fujita, H. Tonami, K. Kato, H. Iwata, S.H. Hsu, Cell orientation and regulation of cell-cell communication in human mesenchymal stem cells on different patterns of electrospun fibers, Biomedical Materials (Bristol) 8 (2013), https://doi.org/10.1088/1748-6041/8/5/055002.
[48] A.A. Bulysheva, G.L. Bowlin, A.J. Klingelhutz, W.A. Yeudall, Low-temperature electrospun silk scaffold for in vitro mucosal modeling, J. Biomed. Mater. Res. 100 A (2012) 757–767, https://doi.org/10.1002/jbm.a.33288.
[49] F.A. Sheikh, H.W. Ju, J.M. Lee, B.M. Moon, H.J. Park, O.J. Lee, J.H. Kim, D.K. Kim, C.H. Park, 3D electrospun silk fibroin nanofibers for fabrication of artificial skin, Nanomedicine 11 (2015) 681–691, https://doi.org/10.1016/j.nano.2014.11.007.
[50] A. Crupi, A. Costa, A. Tarnok, S. Melzer, L. Teodori, Inflammation in tissue engineering: the janus between engraftment and rejection, Eur. J. Immunol. 45 (2015) 3222–3236, https://doi.org/10.1002/eji.201545818.
[51] K. Garg, N.A. Pullen, C.A. Oskeritzian, J.J. Ryan, G.L. Bowlin, Macrophage functional polarization (M1/M2) in response to varying fiber and pore dimensions of electrospun scaffolds, Biomaterials 34 (2013) 4439–4451, https://doi.org/10.1016/j.biomaterials.2013.02.065.
[52] X. Dong, S. Liu, Y. Yang, S. Gao, W. Li, J. Cao, Y. Wan, Z. Huang, G. Fan, Q. Chen, et al., Aligned microfiber-induced macrophage polarization to guide schwann-cell-enabled peripheral nerve regeneration, Biomaterials 272 (2021), https://doi.org/10.1016/j.biomaterials.2021.120767.
[53] Z. Wang, Y. Cui, J. Wang, X. Yang, Y. Wu, K. Wang, X. Gao, D. Li, Y. Li, X.L. Zheng, et al., The effect of thick fibers and large pores of electrospun poly (ε-caprolactone) vascular grafts on macrophage polarization and arterial regeneration, Biomaterials 35 (2014) 5700–5710, https://doi.org/10.1016/j.biomaterials.2014.03.078.
[54] A. Viola, F. Munari, R. Sánchez-Rodríguez, T. Scolaro, A. Castegna, The metabolic signature of macrophage responses, Front. Immunol. 10 (2019).
[55] K.P. Fuller, D. Gaspar, L.M. Delgado, A. Pandit, D.I. Zeugolis, Influence of porosity and pore shape on structural, mechanical and biological properties of poly ϵ-caprolactone electro-spun fibrous scaffolds, Nanomedicine 11 (2016) 1031–1040, https://doi.org/10.2217/nnm.16.21.
[56] M. Daigneault, J.A. Preston, H.M. Marriott, M.K.B. Whyte, D.H. Dockrell, The identification of markers of macrophage differentiation in PMA-stimulated THP-1 cells and monocyte-derived macrophages, PLoS One 5 (2010), https://doi.org/10.1371/journal.pone.0008668.
[57] A.V. Kurynina, M.V. Erokhina, O.A. Makarevich, V.Y. Sysoeva, L.N. Lepekha, S.A. Kuznetsov, G.E. Onishchenko, Plasticity of human THP–1 cell phagocytic activity during macrophagic differentiation, Biochemistry (Moscow) 83 (2018) 200–214, https://doi.org/10.1134/S0006297918030021.
[58] D.J. Crouch, C.M. Sheridan, J.G. Behnsen, R.A. D'Sa, L.A. Bosworth, Cryo-electrospinning generates highly porous fiber scaffolds which improves trabecular meshwork cell infiltration, J. Funct. Biomater. 14 (2023) 490, https://doi.org/10.3390/jfb14100490.
[59] M.F. Leong, W.Y. Chan, K.S. Chian, Cryogenic electrospinning: proposed mechanism, process parameters and its use in engineering of bilayered tissue structures, Nanomedicine 8 (2013) 555–566, https://doi.org/10.2217/nnm.13.39.
[60] M. Xue, C.J. Jackson, Extracellular matrix reorganization during wound healing and its impact on abnormal scarring, Adv. Wound Care 4 (2015) 119–136, https://doi.org/10.1089/wound.2013.0485.
[61] H. Bi, T. Feng, B. Li, Y. Han, In vitro and in vivo comparison study of electrospun PLA and PLA/PVA/SA fiber membranes for wound healing, Polymers 12 (2020), https://doi.org/10.3390/POLYM12040839.
[62] K. Sharma, A. Bullock, D. Ralston, S. Macneil, Development of a one-step approach for the reconstruction of full thickness skin defects using minced split thickness skin grafts and biodegradable synthetic scaffolds as a dermal substitute, Burns 40 (2014) 957–965, https://doi.org/10.1016/j.burns.2013.09.026.

Abbreviations:

ECM –: Extracellular matrix
DMEM –: Dulbecco's modified eagle's medium
DMSO –: Dimethyl sulfoxide
FBS –: Fetal bovine serum
PBS –: Phosphate buffer saline
PCL –: Polycaprolactone
PEO –: Polyethylene oxide
PLA –: Polylactic acid
PMA –: phorbol 12-myristate 13-acetate
SEM –: Scanning electron microscopy